Available online at www.sciencedirect.com
ScienceDirect
Journal of the European Ceramic Society 31 (2011) 1905–1913
www.elsevier.com/locate/jeurceramsoc

Combustion synthesis of doped nanocrystalline ZnO powders for varistors applications

K. Hembram *, D. Sivaprahasam, T.N. Rao [1]

International Advanced Research Center for Powder Metallurgy & New Materials (ARCI), Balapur PO, Hyderabad 50000, AP, India

Received 24 January 2011; received in revised form 29 March 2011; accepted 3 April 2011
Available online 29 April 2011

Abstract

Doped nanocrystalline ZnO powders in the size range between 15 and 250 nm were synthesized by chemical combustion method. The powders were characterized for their physical, structural and chemical properties by BET, X-ray diffraction, FESEM, TEM and XPS. These powders were consolidated into dense varistors discs by compaction, sintering and evaluated for their *I–V* characteristics. Post-calcinations of these powders were found to have great influence on the green density and sinterability. The formations of phases after sintering were confirmed by XRD analysis and EDX. The varistor properties have been studied for different calcination temperatures and compositions. Breakdown voltage as high as 9.5 kV/cm and coefficient of nonlinearity 134 were obtained. Leakage current density was found to be ~1.29 μA/cm^2 for a specific composition and condition. These studies demonstrate the feasibility of one step synthesis of doped ZnO nanopowder and their consolidation into ZnO fine grain varistor exhibiting improved performance.

Keywords: Combustion synthesis; Grain boundaries; Electrical properties, ZnO; Varistors

1. Introduction

ZnO varistors are polycrystalline electronic devices whose primary function is to sense and limit transient voltage surges. They have become technologically important devices because of the high nonlinear electrical characteristics with large energy handling capabilities.[1–3] Although, other varistors based on SnO_2,[4] TiO_2,[5] $SrTiO_3$[6] and WO_3[7] etc. are being explored to replace ZnO based varistors, ZnO varistors are the most widely used in several applications from small current electronic circuits to large current transmission lines because of their high non-ohmic behavior in voltage–current characteristics.

The conventional method of making of ZnO varistors involves mixing of ZnO powder with various additives like bismuth oxide, antimony oxide and several transition metal (Co, Mn, Cr, Ni etc.) oxides into a homogeneous mass and pressing followed by liquid phase sintering at 1200–1300 °C. The average grain size of commercial ZnO varistors is in the range of 10–25 μm. Breakdown voltage and coefficient of nonlinearity of these varistors are 2–3 kV/cm and 30–50, respectively.[1–3] It is known that the performance of ZnO varistors can be improved by reducing the grain size, which allows the increased grain boundary per unit volume and improves the breakdown voltage. Another important factor to achieve high performance varistor is to have the dopants distribution homogeneously throughout the grain boundary.[8,9] The only way to achieve these high performance varistors is to start with fine powders such as nanopowders as the starting materials so that fine grains and homogeneous dopants distribution are retained even after sintering. High energy milling, the technique previously used for making fine ZnO and dopants powders is cost intensive. Ever since nanotechnology has become popular, there have been many techniques developed to make nanocrystalline ZnO powders, which include sol–gel,[10] co-precipitation,[11] intensive mechanical milling,[12,13] microemulsion,[14] metallorganic method,[15] spray pyrolysis,[16] solution coating[17–19] and combustion synthesis.[20,21] Among these, the combustion synthesis appears to be the foremost choice when it comes to the large scale economical production of nanopowders.[22] Sousa et al.[20] studied the synthesis of pure and doped ZnO nanopowders by combus-

* Corresponding author. Tel.: +91 40 24441075x408; fax: +91 40 24442699.
E-mail addresses: kaliyan80@gmail.com (K. Hembram), tatanrao@gmail.com (T.N. Rao).
[1] Tel.: +91 4024443170; fax: +91 40 24442699.

0955-2219/$ – see front matter © 2011 Elsevier Ltd. All rights reserved.
doi:10.1016/j.jeurceramsoc.2011.04.005

Table 1
Theoretical density (TD) of individual and mixture, and wt% of oxides starting raw materials consider for this study.

Materials and their T.D.	ZnO (5.60)	Bi_2O_3 (8.9)	Sb_2O_3 (5.58)	Co_3O_4 (6.11)	Cr_2O_3 (5.21)	MnO_2 (5.10)	Density of the mixture (g/cm^3)
88 wt% ZnO	88	5	3.5	1.5	1	1	5.76
18 wt% ZnO	82	7.25	5.25	2.5	1.5	1.5	5.83
76 wt% ZnO	76	10	7	3	2	2	5.92

T.D.: Theoretical Density.

tion method using urea as a fuel and reported achievement of good control over the compositions. However, they did not study the electrical properties. Hwang et al.[21] used the combustion synthesis method to produce ZnO nanopowder using glycerin as the fuel and studied their properties for varistor applications. They have reported a breakdown voltage 2.05 kV/cm, coefficient of nonlinearity of 42 and a leakage current of 1.15 μA. Varistors made from the above mentioned ZnO nanopowders have not exhibited significant superiority in breakdown voltage, coefficient of nonlinearity and leakage current compared to commercial varistors. Therefore, it is essential and immediate necessity to make superior varistors compared to conventional varistors by using cost effective methods.

In the present investigation, a single step chemical combustion synthesis process has been used to make doped nanocrystalline ZnO nanopowder for varistor applications using sucrose as a fuel. The process is simple, suitable for industrial scale production and involves short processing time. The doped nanocrystalline ZnO powders were compacted, sintered into dense discs and evaluated for various electrical properties like breakdown voltage, coefficient of nonlinearity and leakage current density. Effect of calcination temperatures and composition of the powders on electrical properties have been discussed.

2. Experimental

2.1. Doped nanocrystalline ZnO powder preparation and fabrication of varistors

$Zn(NO_3)_2{\cdot}6H_2O$ (LR, Loba), $Co(NO_3)_2{\cdot}6H_2O$(LR, Loba), $Cr(NO_3)_3{\cdot}9H_2O$ (LR, Loba) and $Mn(NO_3)_2{\cdot}6H_2O$ (LR, Aldrich) were dissolved in D.M. water. The mixture of precursor was heated to 50–80 °C to make a transparent solution (Solution 1). Other two solutions were made by dissolving Sb_2O_3 (LR, Qualigens) in citric acid (LR, SD fine) (solution 2) and Bi $(NO_3)_3{\cdot}5H_2O$ [Loba, LR] in diluted nitric acid [AR, Renkem] (solution 3), respectively. These two solutions were mixed with solution 1. Sucrose (AR, Renkem) was added as a fuel to the final solution. The resulting final solution was heated to 150–250 °C and stirred till the solution dried up. Doped nanocrystalline ZnO powders of different compositions (88, 82 and 76 wt% of ZnO) were prepared. Table 1 shows the percentages of various phases of the constituents' present and their respective densities used for this study. The chemical precursor to fuels ratio have been calculated as reported elsewhere.[21]

The as synthesized powders were calcined at 550 (*550-1 h*), 700 (*700-1 h*) and 750 °C (*750-1 h*) for 1 h and used for comparative studies. Green compact discs were made after mixing the powder with 1.5 wt% PVA by pot milling. The powders were compacted into discs in a 20 mm diameter steel die at 160 MPa pressure by 40 tons hydraulic press. The compacted discs were sintered by a two step sintering method as shown in Fig. 1. Four sintering cycles were used in 100 °C intervals, keeping the heating rate and cooling rates at 2 °C/min and constant holding time to study the densification and grain growth of doped nanocrystalline ZnO powders. Silver paste was applied to both faces of the sintered discs as contact and heat treated at 600 °C for 1 h. The circumference of the sintered disc was covered by insulating materials as reported elsewhere.[23]

2.2. Characterization

The formation of phases of the doped nanocrystalline ZnO powders was characterized by XRD (Bruker D8 advance sys-

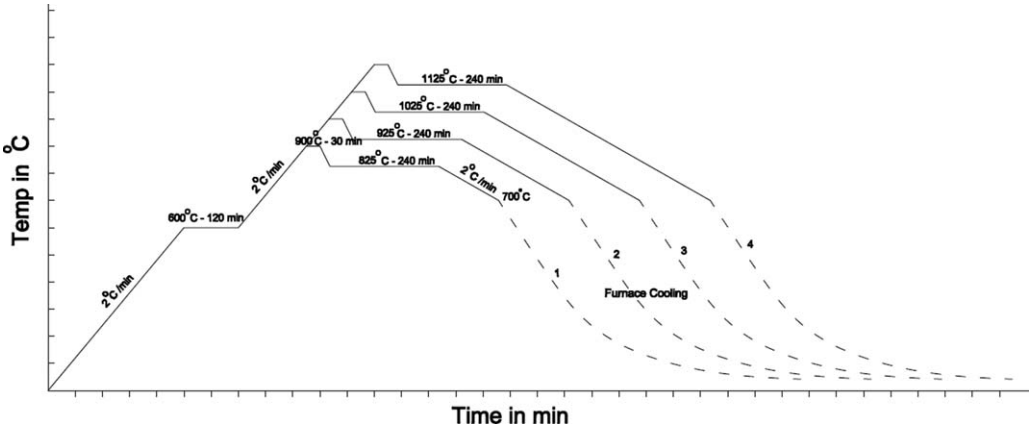

Fig. 1. Schematic diagram of two step sintering cycles followed for the study.

tem) using Cu K_α radiation. The mean grain size (d) of doped nanocrystalline ZnO powders was calculated by using Scherrer formula

$$d = \frac{0.9\lambda}{B\cos\theta} \quad (1)$$

where λ is X-ray wavelength, θ is Bragg angle and B is line broadening, respectively. The line broadening B was measured for the peak (1 0 1) at full width at half maximum (FWHM). The BET surface areas of the powders were measured using a surface area and porosity analyzer (Micromeritics ASAP 2020). Particle sizes were calculated by using formula $d = 6/(s\,\rho)$, where d is the particle diameter, 's' is the surface area and 'ρ' is the theoretical density of the material, respectively. The mean particle size and size distribution of the powders were measured from field emission scanning electron microscopy (FESEM S-4300-SE/N, Hitchi, Japan) and TEM (TECNAI-200 KV, FEI Netherlands) micrographs. The surface characteristics of the doped nanocrystalline ZnO powders were investigated using XPS (Omicron Nanotechnology, UK).

The densities of the green compacts were measured from weight and dimensions method. Densities of sintered discs were measured by Archimedes (Mettler balance & attachment, AG245, Mettler Toledo, Switzerland) method. Polished and thermally etched (900 °C for 15 min) microstructures of the sintered discs were analyzed by FESEM. Compositional elemental analysis of constituent phases present in the microstructure (fracture surface) of sintered discs were carried out by EDS attached to FESEM (EDAX, USA). The average grain size of the ZnO was quantified using image analyzer (Image proplus) by intercept method.

The electrical (I–V) properties of the varistors were measured by DC high voltage tester (Rectifier Electronics, Delhi, India). The coefficient of nonlinearity (α) was defined as follows

$$\alpha = \frac{\log J_2 - \log J_1}{\log E_2 - \log E_1} \quad (2)$$

$E_2 > E_1$, where E_1 is the voltage at current density J_1 (0.1 mA/cm^2) and E_2 is voltage at current density J_2 (1 mA/cm^2), respectively. Breakdown voltage (E_b) was calculated at a current density of 1 mA/cm^2. Leakage current density was calculated at 75% of the breakdown voltage. The average breakdown voltage per barrier (V_g) is calculated by using the relation $V_g = E_b/d$, where E_b is breakdown voltage and d is average grain size of ZnO.

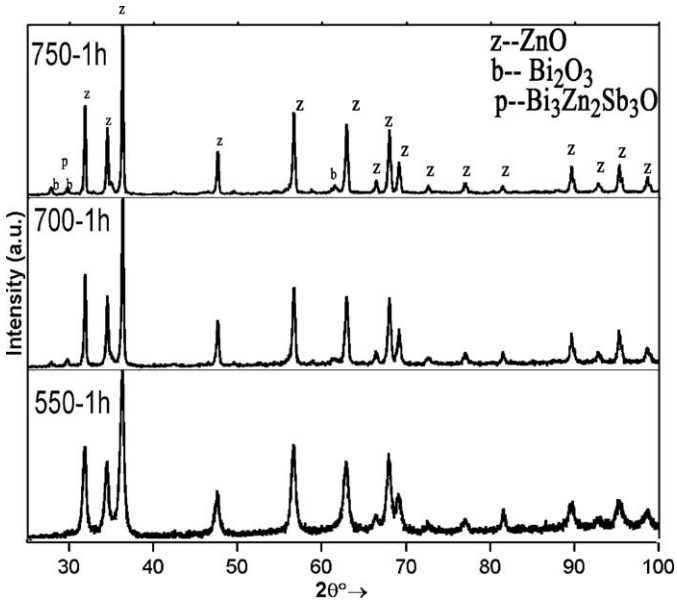

Fig. 2. XRD patterns of doped nanocrystalline ZnO powders of samples 550-*1 h*, *7001 h* and *750-1 h*.

3. Results and discussion

3.1. Doped nanocrystalline ZnO powders

As synthesized ZnO powders were brownish in color. Calcination changed the color of the powders to greenish. Fig. 2 shows the multi-plot XRD patterns of samples *550-1 h, 700-1 h* and *750-1 h*, respectively. In case of the sample *550-1 h*, only pure zincite phase was observed, probably dopants are in amorphous phase and less in amount to detect the X-Ray. However, in case of samples *700-1 h* and *750-1 h*, extra peaks corresponding to the bismuth oxide and $Bi_2Sb_3Zn_2O_{14}$ (pyrochlore) phases were also observed in addition to zincite phase. However, ZnO–Bi_2O_3

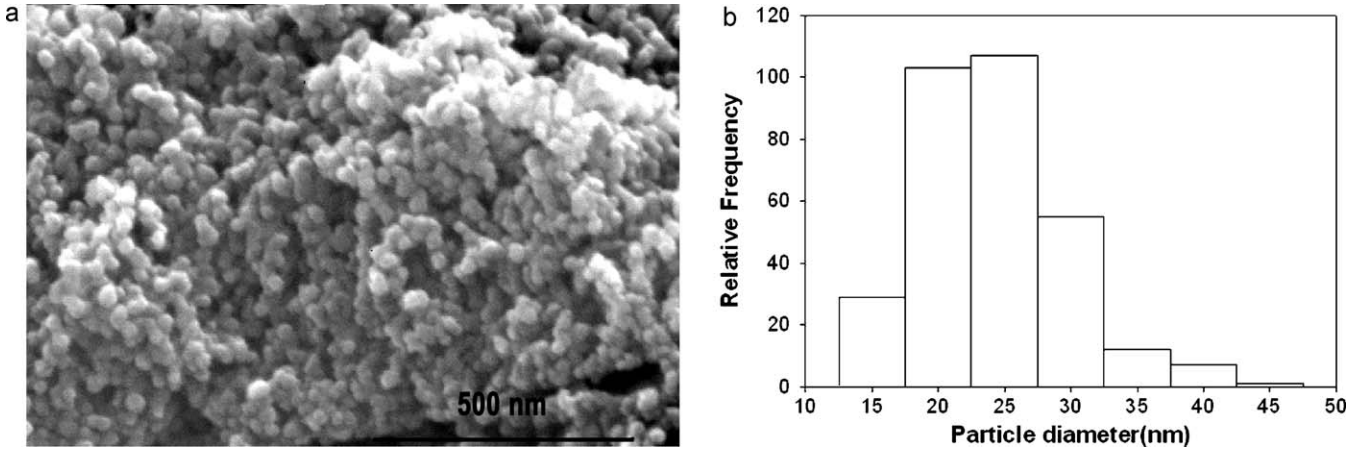

Fig. 3. (a) FESEM image of doped nanocrystalline ZnO powders of sample *550-1 h* and (b) their particles size distribution.

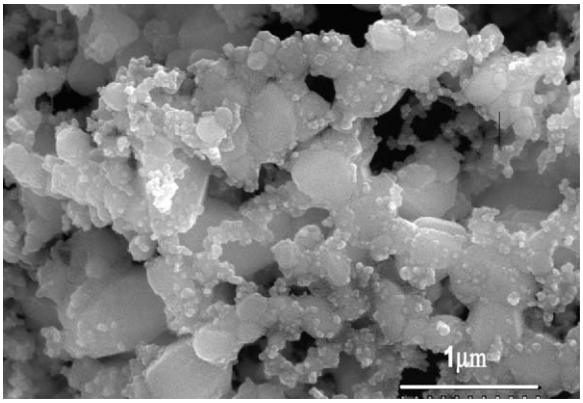

Fig. 4. FESEM image of doped nanocrystalline ZnO powders and dopants precipitates of sample *750-1 h*.

forms eutectic at 735 °C and though, $ZnO–Sb_2O_3$ eutectic temperature is not known, Sb_2O melts at 655 °C.[3] We observed pyrochlore phase formation at 700 °C, generally pyrochlore phase formation is expected at above 700 °C. Eutectic temperature dipping may be due to finer particle size of ZnO and dopants. We observed same kind of phase formation below eutectic temperature in our previous work on doped nanocrystalline ZnO powder synthesis by spray pyrolysis method.[12] Fig. 3a and b shows the FESEM image of sample *550-1 h* and corresponding particle size distribution, respectively. The mean particle size was 26 nm and the size distribution was found to be uniform. BET surface area of 46 m^2/g (particle size 22 nm) and a crystallite size of 18 nm (measured by XRD) were obtained. Fig. 4 shows the FESEM image of sample *750-1 h*. In this case, substantial amount of sintering and growth of doped ZnO particles were observed. The average particle size was 250 nm (FESEM) and the BET surface area was 10 m^2/g. Fig. 5a–c exhibits the bright filed TEM micrographs of doped ZnO nanopowder of samples *550-1 h*, *700-1 h* and *750-1 h*, respectively. From bright field TEM images, we can see clearly that, in case samples *550-1 h* (25 nm) and *700-1 h* (60 nm) for the doped nanocrystalline ZnO powders, there were no secondary phases presents at all. However, in case of sample *750-1 h* the doped ZnO were observed which were made from clusters of several smaller ZnO grains sintered together. In addition, fine dopants precipitates of less than 5–10 nm were present throughout the surface of the doped nanocrystalline ZnO powder. It is interesting to note that in case of sample *700-1 h* on the doped nanocrystalline ZnO powder second phases precipitates were not observed in TEM micrograph. However, XRD pattern of same sample *700-1 h* shows the bismuth and pyrochlore phases. Probably monolayers of secondary phases and dopants are present on the surface of doped nanocrystalline ZnO powders but could not be seen in TEM. This lead us to study the surface chemistry of doped nanocrystalline ZnO powder calcined at different temperatures by using XPS.

Fig. 6a shows XPS comparative spectra of doped nanocrystalline ZnO powders of samples *550-1 h* and *750-1 h*. The surface chemistry of the powder sample revealed the presence of ZnO, Bi_2O_3, Sb_2O_3 and Cr_2O_3. However, no traces of Mn and Co oxide or metal ions were observed. The Zn^{2+} ions may have

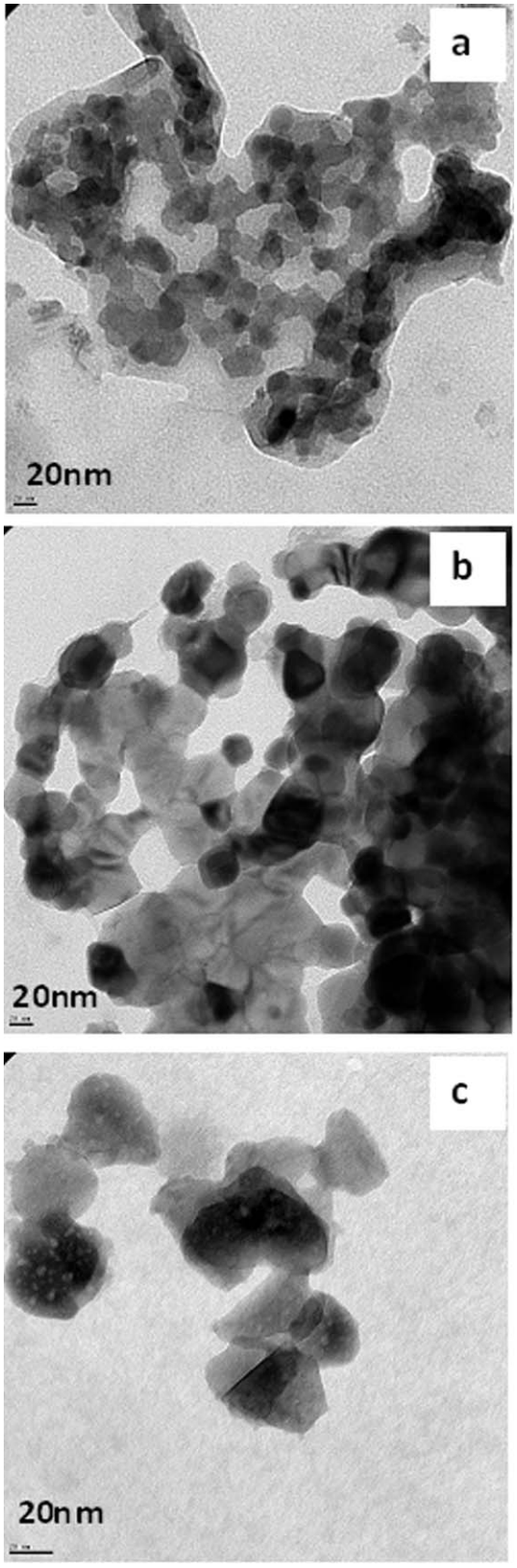

Fig. 5. Bright field TEM images of doped nanocrystalline ZnO powders of samples *550-1 h*, *700-1 h* and *750-1 h* (precipitates on the ZnO grains).

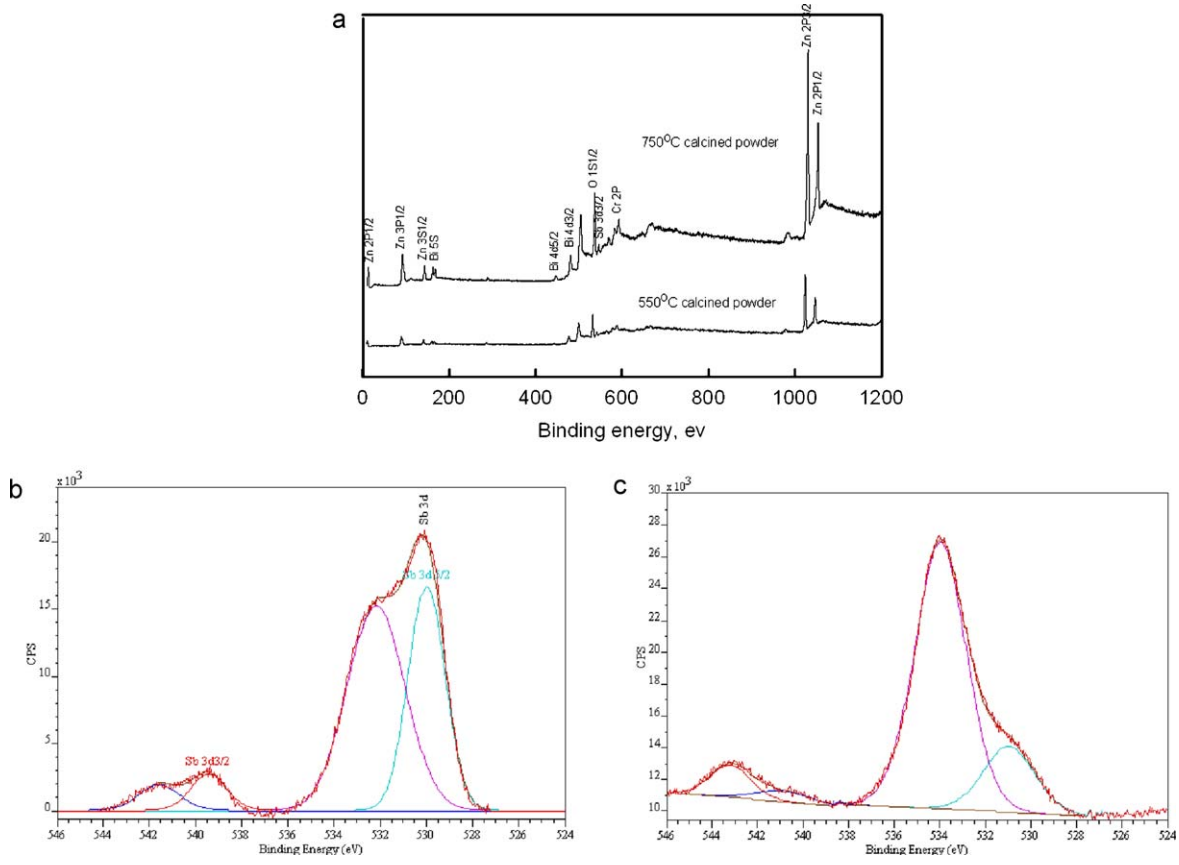

Fig. 6. (a) XPS spectra comparison of doped nanocrystalline ZnO powder of samples *550-1 h* and *750-1 h*, (b) and (c) close view of antimony oxide.

been replaced by Mn^{2+} and Co^{2+} ions in the lattice of ZnO grain. In case of sample *750-1 h,* the spectra of oxides of Zn, Bi and Sb shifted towards the higher binding energy compared to those of the sample *550-1 h*. Fig. 6b and c shows the XPS spectra of samples *550-1 h* and *750-1 h*, respectively. A shift in the binding energy to a higher value may be due to more oxidation on the powder surface and pyrochlore phase formation can be clearly seen. However, no change was observed in Cr_2O_3 XPS spectra of doped nanocrystalline ZnO powders of both samples *550-1 h* and *750-1 h.* It may be due to fact that Cr_2O_3 is completely oxidized even at lower temperature and also directly not taking part in pyrochlore phase formation during the process.

3.2. Compaction and Sintering

The doped nanocrystalline ZnO powders of samples *550-1 h* and *750-1 h* were compacted by uni-axial compaction, resulting in 35–45% and 60–65% of theoretical density, respectively. Most of the green discs made from sample *550-1 h* were laminated during ejection, however, these problems were completely absent in the sample *750-1 h*. Lamination in the green discs in case of the sample *550-1 h* resulted in poor green strength and density. Since the size of the doped nanocrystalline ZnO powder was very small (26 nm) with a very high surface area (46 m^2/g), the friction between nanoparticles is expected to be very high. Additionally, other forces due to electrostatic, van der Walls interaction and surface absorption also become much more significant as particle size decrease to nanolevel.[24] During compaction, these forces significantly influence the densification particularly at lower pressure. In case of the sample *750-1 h* the particle size increased and the surface area decreased significantly resulting in better compactability. It is well known that ≈60% of green density of the theoretical value is desirable to obtain the best sintered density. During ZnO–Bi_2O_3 liquid phase sintering rapid elimination of the porosity is achieved and number of contact points of the ZnO grains increased.[25]

Fig. 7 shows the XRD spectra of 82 wt% ZnO sintered sample (sintering by cycle 2). The δ-Bi_2O_3, $Bi_2Sb_3Zn_2O_{14}$ (Pyrochlore) and β-$Zn_7Sb_2O_{12}$ (spinel) phases were observed. Pyrochlore formation takes place by decomposition of ZnO, Sb_2O_3 and Bi_2O_3 at temperatures in the range of 700–900 °C, while, Spinel and bismuth oxide formation take place by decomposition of zinc oxide and pyrochlore at temperatures in the range of 900–1050 °C by reactions[26]

$$2ZnO + \frac{3}{2}Sb_2O_3 + \frac{3}{2}Bi_2O_3 + \frac{3}{2}O_2 \underset{700–900^\circ C}{\longrightarrow} Zn_2Bi_3Sb_3O_{14} \quad (3)$$

$$2Zn_2Bi_3Sb_3O_{14} + 17ZnO \underset{900–1050^\circ C}{\longrightarrow} 3Zn_7Sb_2O_{12} + 3Bi_2O_3 \quad (4)$$

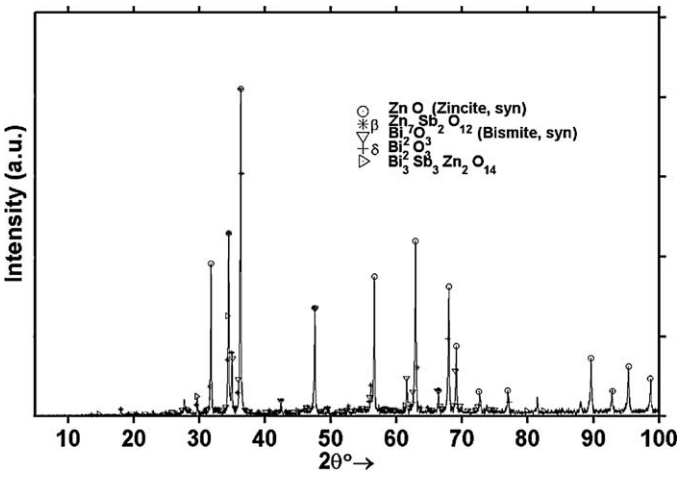

Fig. 7. XRD pattern of 82 wt% ZnO varistor sintered by sintering cycle 2.

Bi_2O_3 helps in densification and for wetting of ZnO grains. $Bi_2Sb_3Zn_2O_{14}$ (Pyrochlore) and β-$Zn_7Sb_2O_{12}$ (spinel) phases are useful for restricting the ZnO grain to grow. Generally, $Zn_7Sb_2O_{12}$ are present in triple junction as well as inside the ZnO grains in the form of inverse grain boundary.[27] As the number of grains increases per unit thickness, the varistor breakdown voltage increases. However, direct relationship with other electrical properties has not been well understood so far.

Fig. 8 shows the fracture surface FESEM image and EDX spectra of (a) bismuth rich phase (brighter area), (b) triple junction (small precipitates) and (c) ZnO grain of 82 wt% ZnO varistor pellet, respectively. At the brighter area the EDX spectra intensity of the Bi was almost equal to the Zn which is the matrix. Other dopants like Sb, Mn, Co and Cr were also observed. Therefore, from the above observation it can be concluded that brighter area of the microstructure might be bismuth oxide rich phase. In the triple junction (small precipitates), the EDX spectra show the presence of Zn, Sb and Bi. It suggested that, the small precipitates are only spinel and pyrochlore phases. In big grains, the EDX spectra have shown the presence of Zn and O indicating that the big grains are composed of ZnO alone.

Fig. 9 shows the FESEM images of polished and thermally etched sintered varistors discs (sample *750-1 h*) of different compositions with (a) 88, (b) 82 and (c) 76 wt% of ZnO, respectively. The microstructures basically contained homogenous mixture of ZnO and second phases. Table 3 shows the ZnO average grain size in the varistor discs of different dopant concentrations. For the sample with less dopant (Bi_2O_3) concentrations, ZnO grain size is smaller than that of higher dopant concentrations. This is because, Bi_2O_3 forms liquid phase during sintering and hence encourages ZnO grains to grow.[25]

The densification and grain growth were studied for the 82 wt% ZnO (sample *750-1 h*) by sintering in different thermal cycles as shown in Fig. 1. The density of sintered discs was increased with increase in sintering temperature to 1025 °C; beyond that decreased due to material loss of Bi_2O_3 by evaporation. It was observed that the grain growth has linear relationship with sintering temperatures. The density of the sintered discs of

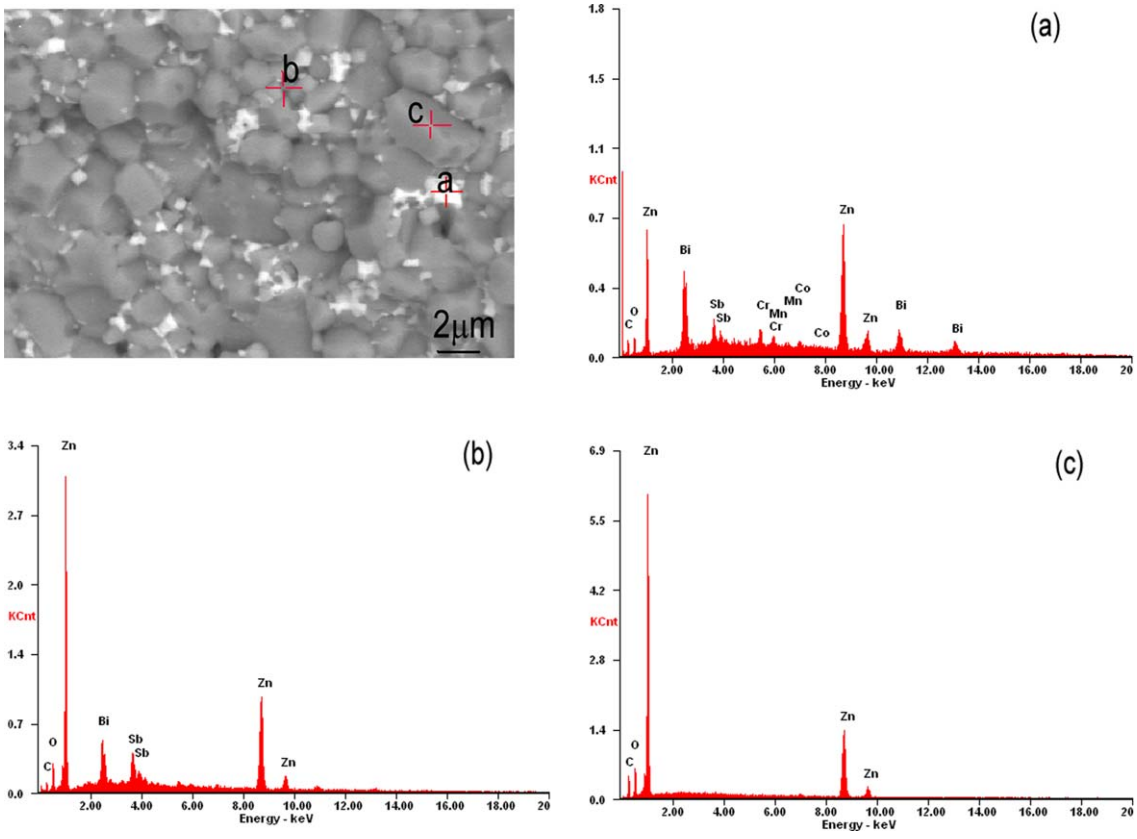

Fig. 8. FESEM image and EDX spectra of 82 wt% ZnO varistor discs conforming (a) bismuth rich phase, (b) pyrochlore and spinel phases and (c) ZnO matrix phase.

Table 2
Doped ZnO nanopowders and varistor discs characteristics of samples 550-*1 h* and *750-1 h* (88 wt% ZnO) sintered by cycle 2.

Sample ID	Surface area (m^2/g)	Average particle size (nm)	G^* (g/cm^3)	S^{**} (g/cm^3)	Average grain size (μm)	E_b (kV/cm)	I_L^{***} ($\mu A/cm^2$)	V_g^+ (V)	α
550 °C–1 h	46	26	2.41	5.49	2.5	9.40	4.98	2.35	134
750 °C–1 h	10	250	3.63	5.61	2.8	8.87	1.67	2.48	112

G^*: green density, S^{**}: sintered density, I_L^{***} : leakage current density, V_g^+ : voltage per barrier, E_b: breakdown voltage, and α: coefficient of nonlinearity.

the sample *550-1 h* was lesser than that of the sample *750-1 h*. This was expected since the green density of discs of the sample *550-1 h* was significantly lower. However, no significant difference was observed in the average grain size of ZnO for both the samples sintered under ideal conditions. This may be due to the fact that the grain growth kinetics of smaller grain is faster compared to that of the larger grain and finally ending up with almost the same grain size. It is interesting to note that the sintered density of the varistor discs increased with increase in the dopants content in spite of the green density follow opposite trend.

3.3. I–V characteristics of varistors discs

Fig. 10 shows the comparison of *I–V* characteristics of varistors made from doped nanocrystalline ZnO of samples *550-1 h* and *750-1 h* (88 wt% ZnO) and Table 2 summarizes the comparative electrical properties of the varistors discs. Breakdown voltages of 9.4 and 8.87 kV/cm and barrier voltage of 2.35 and 2.48 V per grain for varistors made from the samples *550-1 h* and *750-1 h*, respectively, were obtained. This enhancement of breakdown is due to smaller ZnO grain size (∼2.5 μm) in our case compares to commercial 10–25 μm. Coefficient of nonlinearity values were 134 and 112 for the varistors made from the samples *550-1 h* and *750-1 h*, respectively. The coefficient of nonlinearity value obtained in the present work is 2–3 higher than that for earlier reported varistors made from the other combustion synthesis methods.[20,21] This enhancement in coefficient of nonlinearity may be due to better densification of the present samples, which results in better ZnO matrix grain to grain contact, better homogeneous distribution of dopants and lower grain boundary thickness. XPS results indicate that the Co^{2+} and Mn^{2+} have been doped in ZnO grains, which enhance the conductivity of the varistor after breakdown. It is also known that transition metal oxide such as Co and Mn generally improve the coefficient of nonlinearity at lower current density region because of increase in barrier height by trapping of electrons.[28]

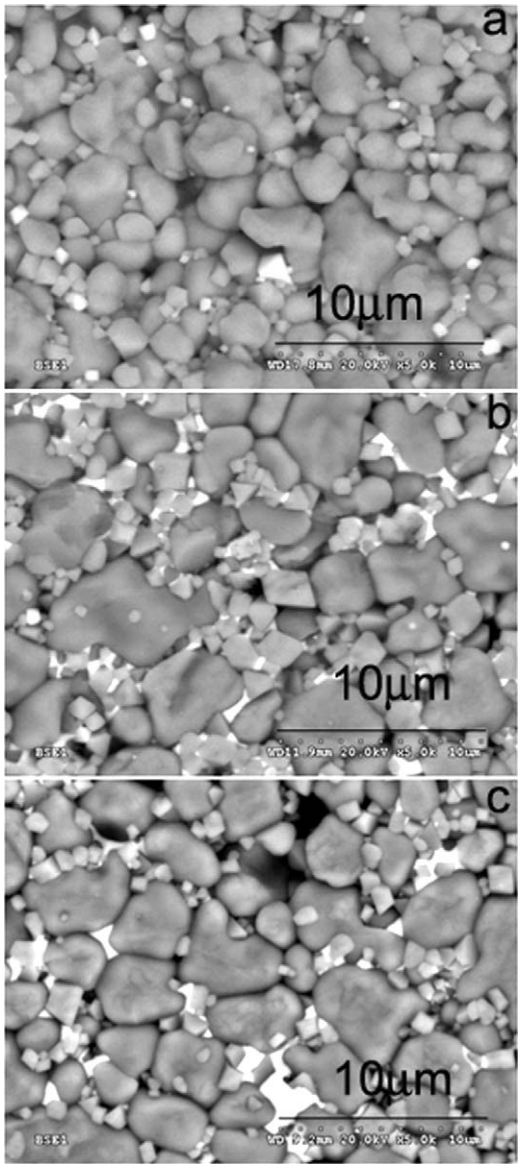

Fig. 9. FESEM images of polished and thermally etched (a) 88 wt% ZnO, (b) 82 wt% ZnO and (c) 76 wt% ZnO varistor discs sintered by cycle 2.

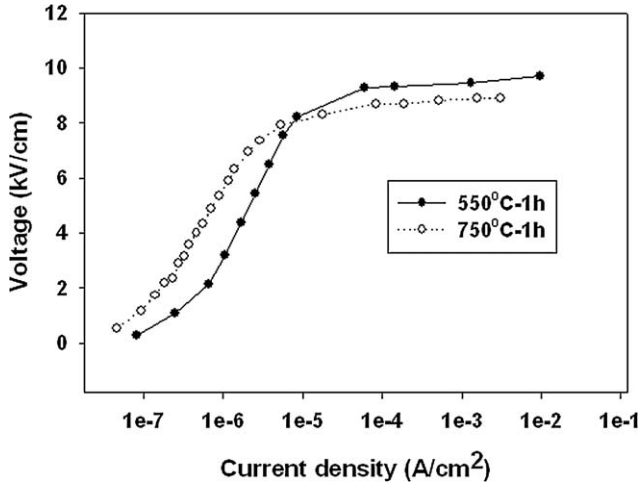

Fig. 10. *I–V* characterization comparison of varistors made (88 wt% ZnO) samples *550-1 h* and *750-1 h* sintered by cycle 2.

Table 3
Varistor discs characteristics of different compositions 88, 82 and 76 wt% ZnO (750-*1 h)* sintered by cycle 2.

Composition	G^* (g/cm^3)	S^{**} (g/cm^3)	Average grain size (μm)	E_b (kV/cm)	I_L^{***} (μA/cm^2)	V_g^+ (V)	α
88 wt% ZnO	3.63	5.61	2.8	8.87	1.67	2.48	112
82 wt% ZnO	3.5	5.66	3.01	7.50	1.29	2.25	56
76 wt% ZnO	2.6	5.71	3.29	6.51	9.68	2.14	27

In the present samples, the possible conduction mechanism of varistor action corresponding to the highly non-linearity above break down voltage may be the combination of space-charge-limited-current and tunneling. The tunneling mechanism is usually less possible in conventional commercial samples (grain size 20 μm) due to its thick grain boundary layer of more than 500 Å, as the tunneling requires a segregation layer with a thickness less than 100 Å.[1,29,30] Assuming the a varistor disc size with diameter of 2 cm and thickness of 1 cm, the total volume of the disc is estimated to be 3.141 cm^3. Considering the grains to be in cubic shape, the volume of 2.5 μm (our sample in the present work) and 20 μm (conventional commercial sample) ZnO grains are estimated to be 15.63×10^{-12} cm^3 and 80.63×10^{-12} cm^3, respectively. Accordingly, the number of grains present per unit volume our sample and commercial sample is 20×10^{10} and 39×10^7, respectively with corresponding surface areas 37.5×10^{-8} cm^2 and 2400×10^{-8} cm^2. This corresponds to total grain boundary area of 75,000 cm^2 and 9360 cm^2 for our sample and commercial sample, respectively, indicating that the total surface areas of our sample is 8 times higher than that of commercial one. Therefore, considering the dopants used for the commercial and in this study are same, the segregation layer thickness of our sample is expected to be lowered by 8 times corresponding to ~62.5 Å. From above assumption and calculation, we can say that the tunneling mechanism of conduction is very much possible in our varistor samples which is significantly contributing in addition to space charge limited current flow. A detailed study based on controlled grain boundary layer thickness to support the above conclusion is in progress.

Fig. 11 shows the comparative *I–V* characteristics of varistors discs of 88, 82 and 76 wt% ZnO (sample *750-1 h*) and

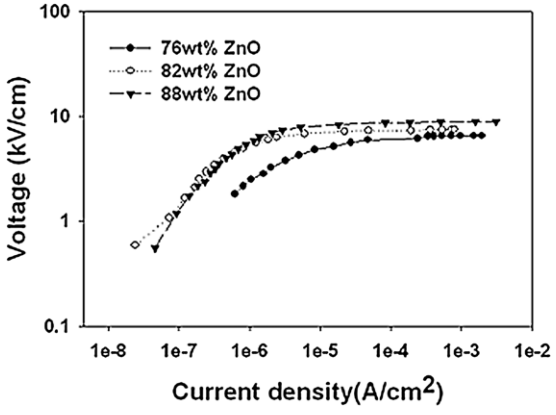

Fig. 11. *I–V* characterization comparison of varistors 88 wt% ZnO, 82 wt% ZnO and 76 wt% ZnO sintered by sintering cycle 2.

Table 3 summarizes value of various properties. It can be clearly observed that the breakdown voltage is coming down with respect to the increase in amount of dopants, while the coefficient of nonlinearity is decreasing. FESEM image shows that more secondary phase is present in case of 76 wt% ZnO varistor and also, sitting on the ZnO grain compared to 88 and 82 wt% ZnO varistors. Deterioration of electrical properties might be due to the amount of secondary phases present around the grain boundary which are more, hence the electron movement decreases.[22] It is know that, a few nanometer thick Bi_2O_3 amorphous phase is responsible for schottky barriers and other phases like pyrochlore and spinel are useful to restrict the ZnO grain to grow. Also, it may be due to the fact that the amount of additives required to cover each grain boundary and partial substitution of Zn^{+2} lattice by Co^{+2} and Mn^{+2} ions in 88 and 82 wt% ZnO varistors were sufficient to obtain better combination of electrical properties. The leakage current density in case of lower dopants (88 and 82 wt% ZnO) varistors was comparable. However, as the dopants concentration increased (76 wt% ZnO), the leakage current density was found to increase abnormally. We did not see any enhancement in the electrical properties due to extra addition of dopants as reported earlier by Zhang et al.[31]

4. Conclusions

Doped nanocrystalline (15–250 nm) ZnO powders were synthesized by chemical combustion method. The pre-calcination temperature of powders was found to have great influence on the green density and sinterability of the varistor discs. A breakdown voltage as high as 9.4 kV/cm and a coefficient of nonlinearity as high as 134 were obtained from the varistor made at certain conditions (powder calcined at 550 °C–1 h of composition 88 wt% ZnO). We demonstrate the highest coefficient of nonlinearity value (134) for the varistor made from doped nanocrystalline ZnO by combustion method. Whereas, the leakage current density as low as ~1.29 μA/cm^2 was obtained for the varistors made from powder calcined at 750 °C–1 h for composition 82 wt% ZnO. As the dopants concentrations were increased, the electrical properties including breakdown voltage and coefficient of nonlinearity slowly deteriorated.

Acknowledgements

Authors like to thank Dr. G.V.N. Rao for helping in analysis of XRD patterns, Dr. Neha Habalkar, for carrying out TEM analysis, L. Ventatesh for carry out FESEM, D. Srinivasa Rao for assisting in experimental works, Dr. S. Dhage for valuable discussions and suggestions, and Dr. B.V. Sarada for helping preparation of manuscript.

References

1. Matsuoka M. Nonohmic properties of zinc oxide ceramics. *Japanese Journal of Applied Physics* 1971;**10**:736–46.
2. Gupta TK. Application of zinc oxide varistors. *Journal American Ceramics Society* 1990;**73**:1817–40.
3. Clarke DR. Varistor ceramics. *Journal American Ceramics Society* 1999;**82**:485–502.
4. Pianaro SA, Bueno PR, Longo E, Varela JA. A new SnO_2-based varistor system. *Journal of Materials Science Letters* 1995;**14**:692–4.
5. Yan MF, Rhodes WW. Preparation and properties of TiO_2 varistors. *Applied Physics Letter* 1982;**40**:356–537.
6. Kutty TRN, Philip S. Low voltage varistors based on $SrTiO_3$ ceramics. *Materials Science and Engineering B* 1995;**33**:58–66.
7. Wang Y, Yao KL, Liu ZL. Novel nonlinear current–voltage characteristics of sintered tungsten oxide. *Journal of Materials Science Letters* 2001;**20**:1741–3.
8. Macary BLS, Kahn ML, Estournés C, Fau P, Trémouilles D, Bafleur M, Renaud P, Chaudret B. Size effect on properties of varistors made from zinc oxide nanoparticles through low temperature spark plasma sintering. *Advanced Functional Materials* 2009;**19**:1775–83.
9. Duran P, Capel F, Tartaj J, Moure C. A strategic two-stage low-temperature thermal processing leading to fully dense and fine-grained doped-ZnO varistors. *Advanced Materials* 2002;**14**:137–41.
10. Pillai SC, Kelly JM, McCormack DE, O'Brien P, Ramesh R. The effect of processing condition on varistor prepared from nanocrystalline ZnO. *Journal of Material Chemistry* 2003;**13**:2586–90.
11. Viswanath RN, Ramasamy S, Ramamoorthy R, Jayavel P, Nagarajan T. Preparation and characterization of nanocrystalline ZnO based materials for varistor application. *Nanostructured Materials* 1995;**6**: 993–6.
12. Schulz R, Boily S, Joly A, Neste AV, Alamdari H, Varistor based on nanocrystalline powder produced by mechanical grinding, US patent: US6 620346B1, 16 September 2003.
13. Fah CP, Wang J. Effect of high-energy mechanical activation on the microstructure and electrical properties of ZnO-based varistors. *Solid State Ions* 2000;**132**:107–17.
14. Hingorani S, Pillai V, Kumar P, Multani MS, Shah DO. Microemulsion mediated synthesis of zinc-oxide nanoparticles for varistor studies. *Material Research Bulletin* 1993;**28**:103–310.
15. Pedro D, Capel F, Tartaj J, Moure C. Sintering behavior and electrical properties of nanosized doped ZnO powders produced by metal-lorganic polymeric processing. *Journal American Ceramics Society* 2001;**84**:1661–8.
16. Hembram K, Vijay R, Rao YS, Rao TN. Doped nanocrystalline powders for non-linear resistor application by spray pyrolysis method. *Journal of Nanoscience and Nanotechnology* 2009;**9**:4376–82.
17. Seyyed SA, Shahraki MM, Sani MAF, Nemati A, Yousefi A. Microstructural and electrical properties of varistors prepared from coated ZnO nanopowders. *Journal of Material Science: Material Electronic* 2010;**21**:571–7.
18. Shi J, Yunge QC, Huang WY. ZnO varistor manufactured by composite nano-additives. *Materials Science and Engineering B* 2003;**99**:344–7.
19. Banerjee A, Ramamohan TR, Patni MJ. Smart technique for fabrication of zinc oxide varistor. *Material Research Bulletin* 2001;**36**:1259–67.
20. Sousa VC, Segadães AM, Morelli MR, Kiminami RHGA. Combustion synthesized ZnO powders for varistor ceramics. *International Journal of Inorganic Materials* 1999;**1**:235–41.
21. Hwang C-C, Wu TY. Synthesis and characterization of nanocrystalline ZnO powder by a novel combustion synthesis method. *Materials Science and Engineering B* 2004;**111**:197–206.
22. Patil Kashinath C, Aruna ST, Mimani T. Combustion synthesis: an update. *Current Opinion in Solid State and Materials Science* 2002;**6**:507–12.
23. Li S, Li J, Chen G, Davis AE. Interfacial space charge between ZnO varistor ceramics and coating materials. In: *Annual Report Conference on Electrical Insulation and Dielectric Phenomena*. 2002. p. 478–81.
24. Groza JR, Dowding RJ. Nanoparticulate materials densification. *NanoStrutured Materials* 1996;**7**:749–68.
25. Wong J. Sintering and varistor characteristics of ZnO–Bi_2O_3 ceramics. *Journal of Applied Physics* 1980;**8**:4453–9.
26. Inada M. Formation mechanism of nonohmic zinc oxide ceramics. *Japan Journal Applied Physics* 1980;**19**:409–19.
27. Onreabroy W, Sirikulrat N, Brown AP, Hammond C, Milne SJ. Properties and intergranular phase analysis of a ZnO–CoO–Bi_2O_3 varistor. *Solid State Ionics* 2006;**177**:411–20.
28. Kim ED, Kim CH, Oh MH. Role and effect of Co_2O_3 additive on the upturn characteristics of ZnO varistor. *Journal of Applied Physics* 1985;**8**:3231–5.
29. Eda K. Conduction mechanism of non-ohmic zinc oxide ceramics. *Journal of Applied Physics* 1978;**5**:2964–72.
30. Fisher JC, Giaever I. Tunneling through thin insulating layers. *Journal Applied Physics* 1961;**2**:172–7.
31. Zhang J, Cao S, Zhang R, Yu L, Jing C. Effect of fabrication condition on *I–V* properties of ZnO varistor with high concentration additives by sol–gel technique. *Current Applied Physics* 2005;**5**:381–6.